



OPEN ACCESS

EDITED BY

Weiwei Peng,
Shenzhen University, China

REVIEWED BY

Pedro Henrique Martins da Cunha,
University of São Paulo, Brazil
Shirin Madarshahian,
Thomas Jefferson University, United States

*CORRESPONDENCE

David A. Dinsmoor
✉ david.a.dinsmoor@medtronic.com

RECEIVED 14 February 2025

ACCEPTED 30 May 2025

PUBLISHED 30 June 2025

CITATION

Cedeño DL, Vallejo R, Platt DC, Williams JM,
Litvak LM, Dinsmoor DA and Siorek M (2025)
Evolution of spinal evoked compound action
potential thresholds, visual motor
thresholds, and impedances in a rodent
spared nerve injury model.
Front. Neurosci. 19:1577059.
doi: 10.3389/fnins.2025.1577059

COPYRIGHT

© 2025 Cedeño, Vallejo, Platt, Williams,
Litvak, Dinsmoor and Siorek. This is an
open-access article distributed under the
terms of the [Creative Commons Attribution
License \(CC BY\)](https://creativecommons.org/licenses/by/4.0/). The use, distribution or
reproduction in other forums is permitted,
provided the original author(s) and the
copyright owner(s) are credited and that the
original publication in this journal is cited, in
accordance with accepted academic
practice. No use, distribution or reproduction
is permitted which does not comply with
these terms.

Evolution of spinal evoked compound action potential thresholds, visual motor thresholds, and impedances in a rodent spared nerve injury model

David L. Cedeño^{1,2}, Ricardo Vallejo^{1,2,3}, David C. Platt^{1,2},
Joseph M. Williams², Leonid M. Litvak⁴, David A. Dinsmoor^{4*}
and Małgorzata Siorek⁴

¹SGX Medical LLC, Bloomington, IL, United States, ²Illinois Wesleyan University, Bloomington, IL, United States, ³MiVi, Barcelona, Spain, ⁴Medtronic plc, Minneapolis, MN, United States

Introduction: The mechanisms of spinal cord stimulation (SCS) on neuropathic pain are commonly studied using the spared nerve injury (SNI) model, with stimulation amplitudes typically programmed relative to the visual motor threshold (vMT). Recent work explored the relationship between vMTs and spinal evoked compound action potential thresholds (ECAPTs)—a sensed measure of neural activation—in SNI rodents to better translate towards clinical dosing. However, changes across chronic healing beyond two days and pain states is unknown.

Methods: This study tracked ECAPs through a traditional SNI-SCS approach, where nine rats were implanted with an SCS lead to evaluate effects of acute healing (days 0 to 1), chronic healing (days 1 to 7), nerve injury (days 7 to 14), and continuous SCS (days 14 to 16) using differential target multiplexed programming (DTMP).

Results: ECAPT:vMT ratios significantly increased on subsequent recordings from day 0 through day 14 (i.e., post-injury), but not between days 14 and 16 (after SCS), across anesthesia states, or SCS pulse widths. On average, ECAPT:vMT increased from $35 \pm 2\%$ (mean \pm S.E.) on implantation day to $54 \pm 1\%$ on day 16.

Discussion: Future studies may use this approach to further elucidate the effects of chronic pain and SCS on the spinal ECAP.

KEYWORDS

evoked potentials, motor threshold (MT), neuropathic pain (NP), rat model, ECAPS

Introduction

Many preclinical studies exploring the mechanism of action underlying spinal cord stimulation (SCS) therapy leverage the spared nerve injury (SNI) model (Decosterd and Woolf, 2000; Tilley et al., 2015). This model is well-known to induce the mechanical and thermal allodynia that enables the study of the behavioral and neurophysiological effects

of SCS. While some SCS parameters such as rate and pulse width (PW) may be employed identically between humans and preclinical models, delivering an equivalent dose remains a challenge owing to anatomical differences (such as cerebrospinal fluid thickness) across species (Chakravarthy et al., 2020; Cedeño et al., 2023b). Preclinical SCS models have historically titrated stimulation amplitudes to a percentage—such as 90%—of the visual motor threshold (vMT) (Crosby et al., 2015); the vMT is the SCS amplitude for which a muscle contraction is first observed. In contrast, SCS amplitudes in humans are often programmed relative to the patient's perceptual threshold (Al-Kaisy et al., 2020). As such, a significant difference can exist between the extent of neural activation in the preclinical model versus clinical use.

One method to realize equivalent neural activation both clinically and preclinically is to program SCS amplitudes relative to the evoked compound action potential threshold (ECAPT). The ECAPT—a measure of the onset of synchronized neural activation in the dorsal columns—is closely related to the paresthesia threshold in humans (Pilitsis et al., 2021). Previous work has now assessed both ECAPTs and vMTs in rats to provide context around legacy preclinical research that used vMT alone. In initial investigations (Dietz et al., 2022; Cedeño et al., 2023b), healthy, nerve injury-naïve rats were used; more recent work (Versantvoort et al., 2024) included a SNI model up to 2 days after lead implantation. These reports suggest that vMTs occur at approximately 3.0 times greater amplitudes than ECAPTs, a ratio similar to values noted in observational studies of rodents where the sensory threshold occurred at 40–50% of the vMT (Shechter et al., 2013; Song et al., 2014; Cedeño et al., 2023a). Other work has provided additional mechanistic insight into SCS by investigating novel evoked synaptic activity potentials (ESAPs) (Sharma et al., 2023), as well as differentially unique phenomena with low- versus high-rate stimulation (Sagalajev et al., 2024), though these studies were using acute terminal experiments in injury-naïve animals.

While important in elucidating dosing of SCS in translational neuropathic pain models, the aforementioned electrophysiology work in SNI rats only explores ECAPs for up to 2 days post implantation (Dietz et al., 2022; Versantvoort et al., 2024). However, as the acute inflammatory response transition to chronic healing, changes in encapsulation impact impedances (Arle et al., 2014; Garcia-Sandoval et al., 2018; Straka et al., 2018) and thus would likely impact neural activation. Additional translational insights from preclinical models of neuropathic pain may be realized by extending the study duration, with the effects of continuous SCS assessed over multiple days for rats (Tilley et al., 2015; Cedeño et al., 2020, 2023a; Vallejo et al., 2020; Wang et al., 2022) or weeks including larger models such as sheep (Reddy et al., 2018; Cedeno et al., 2022). Moreover, such models should employ lead designs and materials, such as platinum-iridium (Pt-Ir) electrodes, similar to those used clinically; the electrode composition in some prior reports is unfortunately not reported (Dietz et al., 2022; Versantvoort et al., 2024). Assessing the maturation of the electrode-tissue interface and the change in neurophysiological responses over the entire acute and chronic post-surgical interval is an important dimension to this class of work (Salatino et al., 2017; Shepherd et al., 2018; Carnicer-Lombarte et al., 2021).

In this study, the spinal ECAPs of rats—chronically implanted with a cylindrical SCS lead incorporating conventional Pt-Ir

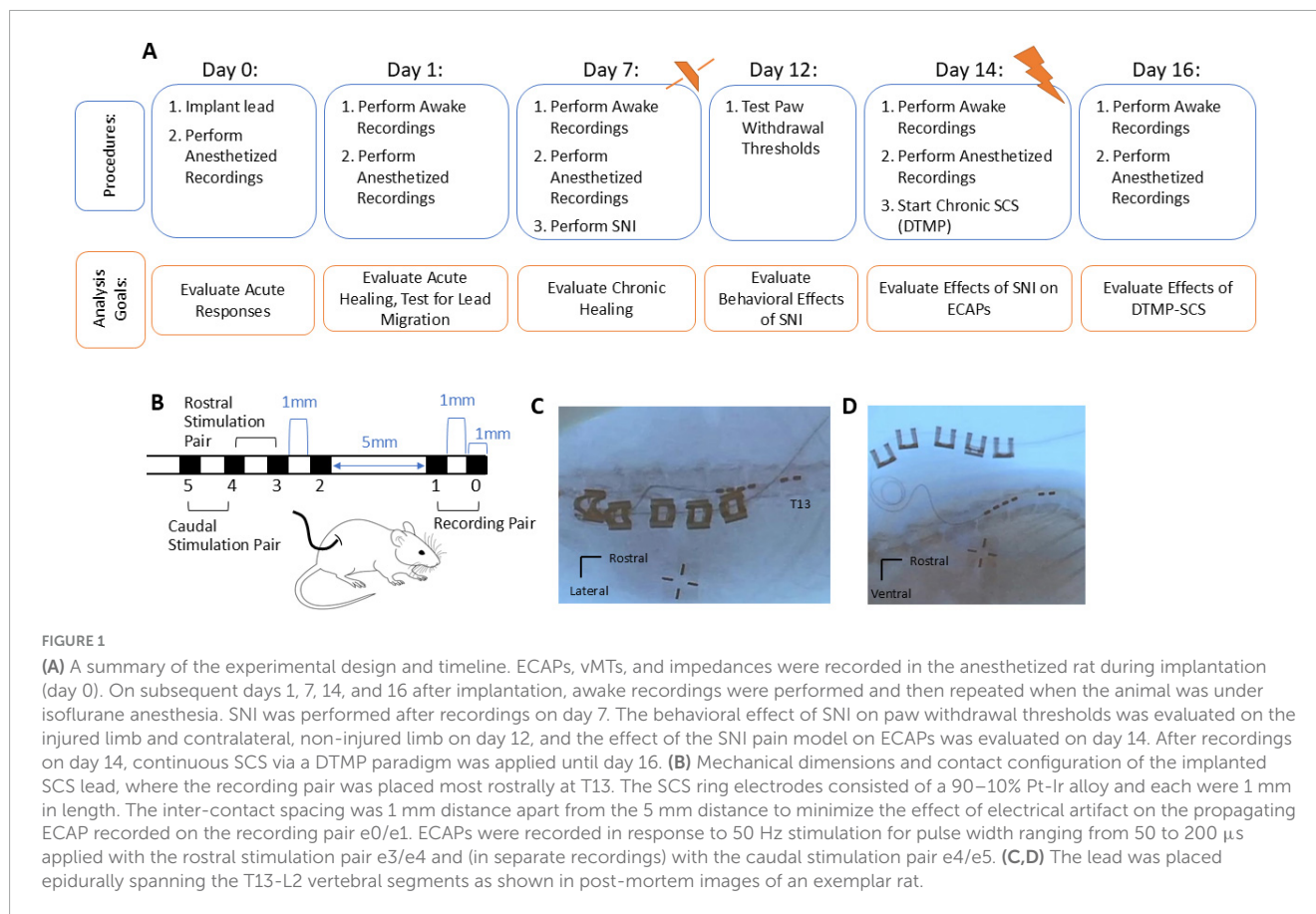
electrodes—were evaluated at multiple time points across a 16-day interval. The ECAPs were in turn related to evoked muscle activity via vMTs. In addition, tissue impedances were characterized longitudinally to evaluate changes in the electrode-tissue interface due to healing. Changes in ECAPs were further explored after inducing the SNI model as well as after continuous SCS, following a common SNI-SCS timeline (Vallejo et al., 2020). For the continuous SCS stimulation from days 14 to 16, DTMP-SCS was delivered as it has been shown to have a larger decrease in mechanical hypersensitivity than low-rate stimulation or high-rate stimulation through modulation of neuron-glia interactions (Cedeño et al., 2020, 2023a; Vallejo et al., 2020).

This longitudinal study approach allowed each animal to serve as its own control prior to the SNI. This study was primarily a feasibility study. We hypothesized we would see changes in neural activation and impedance immediately post implantation, and possibly additional changes after SNI. We did not expect further changes after chronic SCS given prior preclinical experience with continuously applied DTMP-SCS (Cedeno et al., 2022; Cedeño et al., 2023b). Neural activation was characterized via ECAPTs, slope of growth curves, latency, and conduction velocity measurements, and the changes in ECAPTs were related to those of the vMTs. While only recordings on anesthetized animals were performed at the day of implantation, both recordings in awake and anesthetized animals were collected starting on day 1 and onward to investigate the interdependency of anesthesia, time, and chronic pain state.

Materials and methods

Subjects and leads

All procedures were approved by the Institutional Animal Care and Use Committee at Illinois Wesleyan University following NIH guidelines for the ethical use of animal subjects in research. The authors complied with the ARRIVE guidelines. Ten male Sprague-Dawley rats (Envigo, Indianapolis, IN) approximately 12 weeks old weighing in the 297–320 g range at the start of the experiment were used in this study. The sample size used was selected for consistency with prior work (Cedeño et al., 2023b). Before experimental use, animals were housed in pairs in a temperature and humidity-controlled environment with a 12-h light/dark cycle. Food and water were supplied *ad libitum*. After lead implant, each animal was housed individually to prevent other animals from disturbing the external portion of the lead. Environmental conditions were kept similar to pre-implant. Animals were monitored daily for adverse events related to experimental interventions. An on-call veterinarian was available to assist with any serious event, though no such event occurred in the course of the study. Whenever isoflurane anesthesia was delivered, the animal was placed on a hot plate and the temperature was monitored to prevent hypothermia. Immediately after isoflurane, animals were allowed to recover in an empty cage to prevent inhalation of bedding material before returning to their cages. Some practical aspects of the experiment, including placing the reference needle and restraining the animal in a tube to minimize movement artifacts, may have caused the animal some stress and/or minor acute pain in the awake condition.



To minimize this, animals were continuously visually monitored and other experimental interventions (e.g., behavioral testing) was minimized on recording days.

A custom lead [cylindrical hexapolar lead (Oscor Inc., Palm Harbor, FL)] (Figure 1), comprised of 0.65-mm diameter ring electrodes (90–10% Pt-Ir alloy) each 1 mm in length, was implanted in each animal following a previously reported method (Tilley et al., 2015; Vallejo et al., 2020). The custom lead was designed to allow for DTMP-SCS at approximately L1–L3, targets similar to prior studies (Cedeño et al., 2020, 2023a; Vallejo et al., 2020) while also enabling the sensing of orthodromically propagating ECAPs in different recordings. The distal two recording electrodes (e0/e1) had an edge-to-edge spacing of 1 mm, followed by a gap of 5 mm between e1 and e2, with subsequent edge-to-edge spacing of 1 mm between the stimulating electrodes. The 5 mm spacing between recording and stimulating electrodes was selected to limit contamination of stimulation artifact on the ECAP recording (Chakravarthy et al., 2022).

Experimental overview

Figure 1A shows a timeline for procedures and recordings with corresponding analysis goals. Briefly, stimulating electrical pulses (50 Hz) were delivered and both the orthodromically propagating ECAPs and vMTs were recorded. ECAPs were sensed on the recording pair of electrodes (e0/e1) in response to 50 Hz active recharge stimulation using a rostral stimulation pair (e3/e4) and,

in separate recordings, using a caudal stimulation pair (e4/e5) (Figure 1B). On implantation day 0, only recordings under isoflurane anesthesia were performed; in subsequent days (days 1, 7, 14, and 16) recordings were first performed while awake and then under isoflurane anesthetized conditions. For each condition, ECAPs were sensed in response to electrical stimulation that was increased in 5 μ A steps from 0 μ A to just above when motor twitches were observed (vMT). Impedances were collected after recording ECAPs in each condition.

Recordings on day 1 post-implant were taken to evaluate neural activation and lead integrity, as well as check for any lead migration that may have occurred in the early post-surgical interval. In one animal, a notable change in ECAPs was observed at day 1, presumably due to lead migration. This animal was discontinued from the study, and its data excluded in the analysis. For the remaining 9 animals, healing over 1 week was evaluated via recordings on day 7 post-implant. The SNI was performed after recordings on day 7, and paw withdrawal thresholds (PWTs) for mechanical stimulus were collected on day 12 (i.e., 5 days post SNI) to confirm mechanical hypersensitivity associated with the SNI model. The effect of the SNI pain model on ECAPs was evaluated on day 14 post-implant (i.e., 7 days post-SNI). After recordings on day 14 post-implant, continuous DTMP-SCS was applied through day 16 post-implant. Recordings on day 16 assessed the carryover effect of continuous DTMP-SCS—if any—on neural activation.

After study completion, the animals were euthanized via carbon dioxide asphyxiation, and a subset of 5 cadavers were x-ray imaged to assess lead position (see Figures 1C,D for examples). While it

was not possible to collect x-ray images for remaining animals in the study, the lead placement for the first 5 animals was confirmed to be within one vertebral body of the target T13, suggesting that this electrode array configuration and surgical technique enabled consistent placement. All data recorded were subsequently analyzed off-line. Further details are expanded below.

Stimulating/recording and lead impedance measurement systems

A similar experimental setup as described previously (Cedeño et al., 2023b) was used to deliver stimulation and record ECAPs. Stimulation signals were sourced with a waveform generator (Model number 33511B, Keysight Technologies Inc., Santa Rosa, CA) and passed through a constant current stimulation isolator (Model number 2200, A-M Systems Inc., Sequim, WA). ECAPs were amplified (Model number D440, Biopac Inc., Goleta, CA), digitized (Model number MP160, Biopac Inc.) at a sampling rate of 40,000 samples/s, and stored on a laptop computer with recording software (AcqKnowledge v5.0, Biopac Inc.) that enabled streaming visualization of raw signals. The ECAPs were recorded differentially between the two most cranial electrodes (e0/e1) of the lead. Balanced, biphasic pulsed signals with a rate of 50 Hz, PW of 50, 100, 150, or 200 μ s, and amplitudes from 0 μ A to just above vMT in 5 μ A steps were used to elicit ECAPs and vMTs. As each step was increased manually up to vMT, randomization of stimuli was not possible. For each animal, electrical stimuli were delivered on a rostral electrode pair (e3/e4) and, in separate recordings, on a caudal electrode pair (e4/e5). Impedances were recorded using an investigational device (ECHO-MDT, Medtronic plc) between all contacts pairs in response to square pulses at 100 Hz, 75 μ A amplitude, and 80 μ s PW. The influence of anesthesia state, contact configuration, and day after implantation on impedance values were evaluated.

Lead implantation procedure and intraoperative ECAP monitoring (day 0)

The surgical procedure for implanting cylindrical leads in the dorsal epidural space of rats is described elsewhere (Vallejo et al., 2020). Briefly, animals were induced with 4% isoflurane anesthesia, and 3–3.5% isoflurane was maintained throughout the procedure. An incision was made over the lumbar spine, followed by a microlaminectomy at L4 for anterograde implantation of the lead. The lead was introduced through the interlaminar space between L3 and L4 and positioned with the distal tip at T13. An amplifier reference needle (Model number 8227103, Medtronic plc) was placed subcutaneously near the base of the tail. ECAP growth curves, vMTs, and impedances were collected. Lead position was adjusted mediolaterally as needed to optimize ECAP recordings. The proximal cable of the lead was anchored internally in the musculature around the L5 spinous process, and the externalized cable secured to the skin using silk sutures and stainless steel clips. The external portion of the cable was looped within a homemade harness secured around the animal trunk. The reference needle was

removed, anesthetics stopped, and the animal allowed to recover before returning to the colony.

Chronic recordings procedure (day 1–16 post-implant)

Starting day 1 post implantation, recordings were performed first in awake, restrained animals. For these recordings, animals were placed in a tubular rodent holder for 250–500 g animals (Kent Scientific Torrington, CT, United States) with an amplifier reference needle placed subcutaneously near the base of the tail. The ECAPs and vMTs were recorded, followed by the impedance measurement, as described above. Restraining of the awake animal was used to limit variability in the spacing between the electrodes and the cord that might otherwise influence the repeatability of the measurements. After completing awake recordings, the animal was anesthetized as described above, and recordings were repeated to determine the effect, if any, of anesthesia.

SNI procedure (day 7 post-implant)

The SNI procedure (Decosterd and Woolf, 2000; Vallejo et al., 2020) was performed following anesthetized recordings on day 7 post-implantation. This consisted of exposing, under isoflurane anesthesia, the sciatic nerve ipsilateral to motor stimulus at the level of its trifurcation to the sural, peroneal, and tibial branches, transecting and removing 1–2 mm of tissue from the tibial and common peroneal nerves while leaving the sural branch intact. To confirm induction of the SNI, the extent of mechanical sensitization was assessed 5 days after the procedure by measuring the PWTs of the injured and contralateral (non-injured) limbs. These were collected using standard von Frey filaments with an electronic esthesiometer (IITC Life Science, Woodland Hills, CA) (Martinov et al., 2023). We also analyzed the ratio of the two PWTs, where a ratio of 100% would indicate no impairment (i.e., failure of induction) as the limbs have a similar response, and low percentages would indicate high impairment (i.e., success of induction) as the affected limb would not tolerate the mechanical stimulus.

Continuous SCS (day 14–16 post-implant)

Given that DTMP-SCS has shown to significantly decrease mechanical hypersensitivity after 48-hours of continuous stimulation in prior rat studies compared to low-rate stimulation or high-rate stimulation (Vallejo et al., 2020; Cedeño et al., 2023a), DTMP-SCS was continuously delivered after the recordings taken on day 14 though day 16 in a method similar to previous studies (Cedeño et al., 2023a). The electrode cables were connected to an external neurostimulator (ENS, 97725; Medtronic, Minneapolis MN) via a connector block fastened to a custom-made harness. The DTMP approach incorporates 50 Hz stimulation applied on contacts e2e3 with 150 μ s PW, multiplexed with 3 \times 300 Hz stimulation applied at contacts e4e5 with 50 μ s PW. For

consistency with prior reports, stimulation amplitudes were set to approximately 50% vMT at awake conditions on day 14 (range: 10–80 μ A) (Cedeño et al., 2023a). Recordings were performed after SCS on day 16 to evaluate the effect of continuous SCS applied for 2 days.

Data analysis

All data was analyzed off-line using custom software in MATLAB 2020b (Mathworks, Inc., Natick, MA) similar to that used in a previous study (Cedeño et al., 2023b), with some modifications. Briefly, the stimulation artifact was first removed using an exponential modeling method, and then the resulting responses acquired at each stimulation amplitude step were averaged (Figure 2). The amplitude of the ECAP was calculated via the difference between the N1 and P2 features of the averaged polyphasic ECAPs. N1 was defined as the minimum voltage in the window between 0.09 and 0.5 ms after the end of a stimulation pulse, with P2 defined as the maximum voltage in the window between 0.25 and 0.75 ms after a stimulation pulse.

Determination of ECAPTs and vMTs

Growth curves were generated (see Figures 2C,D for examples) for each stimulation amplitude sweep by plotting the measured ECAP amplitudes versus the delivered stimulation current at a fixed PW. From each growth curve, the ECAPT was defined as the x-intercept resulting from fitting a regression line to the first three ECAP magnitudes above a threshold of 10 μ V. If at least three points did not exceed 10 μ V, then a threshold of 5 μ V was used. Additional points were iteratively included for more accuracy if (1) the calculated slope did not decrease by more than 1% or (2) the x-intercept was negative or exceeded the max stimulation amplitude. In addition, the slope of the growth curve from the fit was also characterized.

The stimulation amplitude sweep continued until muscle motion was elicited by the stimulation current. The stimulation current at which this motion was observed was recorded as the vMT. For each growth curve, the ECAPT (Figure 2E for an example) and the concurrent vMT (Figure 2F for an example) were collected. The relationship between these were determined by calculating the ECAPT:vMT ratio (Figure 2G for an example).

Across all animals, 648 growth curves and corresponding ECAPTs were analyzed and visually assessed; 7 of which were manually corrected for accuracy. In addition, one growth curve was excluded from analysis due to partial data being saved for offline analysis. For the remaining 640 growth curves, the 95% Confidence Interval (CI) of individual ECAPTs was estimated using parametric bootstrap as detailed previously (Cedeño et al., 2023b). The slope of each of these 640 growth curves was calculated.

Determination of ECAP latencies and conduction velocities

The ECAP latency was calculated from recordings with the 50 μ s PW stimulation delivered using electrode pairs e3/e4, and separately with pairs e4/e5. By utilizing the shortest PW, the potential for electrical artifact contamination on the ECAP recording was limited. First, the smallest average ECAP with

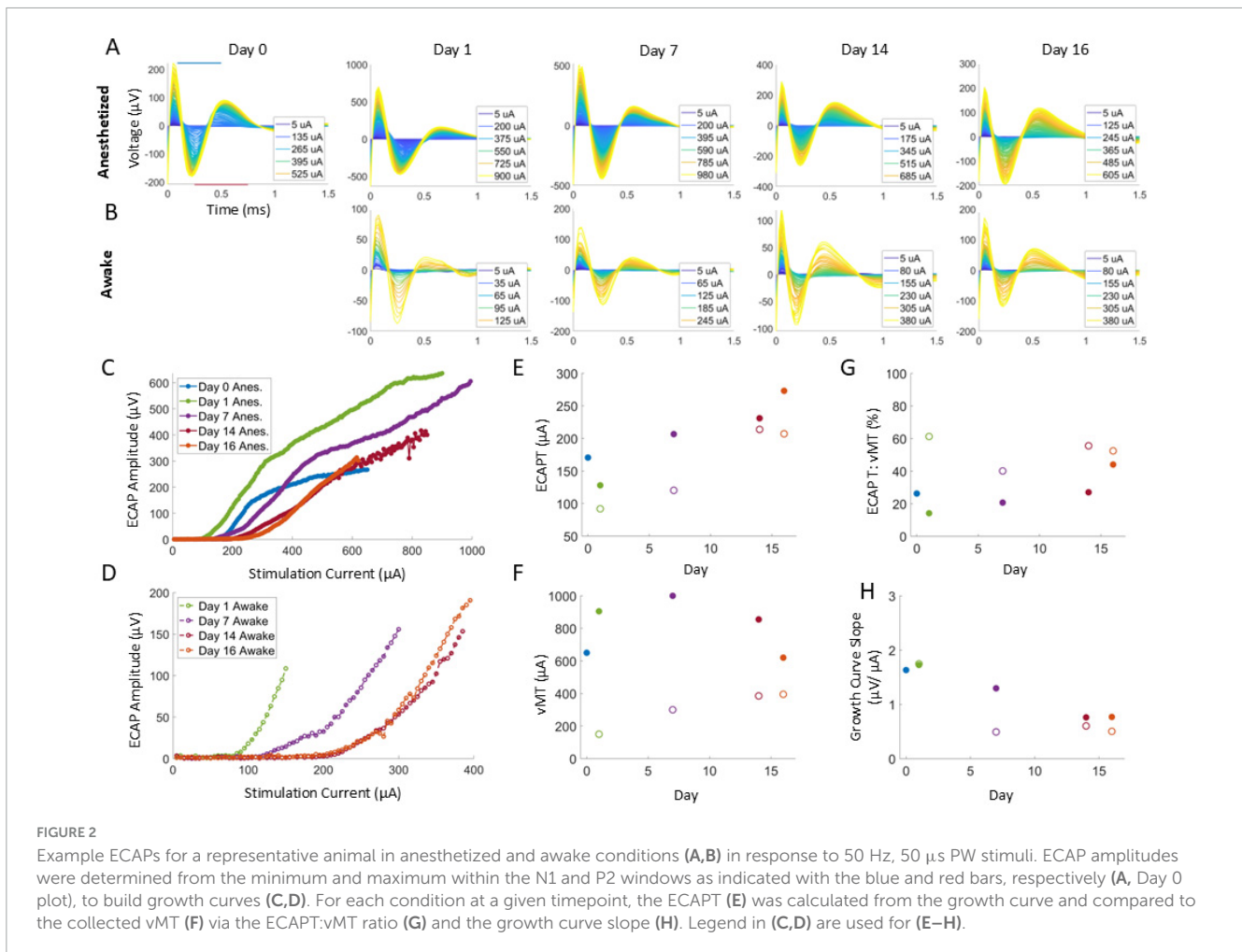
at least a 20 μ V amplitude in each recording was identified. In our recordings, 20 μ V was well above the noise floor of the recording system but consistently below the point where the growth curves saturated as the stimulus amplitude increased. Then, latency was calculated by measuring the interval between the trailing edge of the stimulation pulse and the N1 feature of the 20 μ V ECAP. Finally, we assessed both e3/e4 and e4/e5 latency differences as well as the conduction velocity (defined here as the separation between the proximal edges of e5 and e1 (12 mm) divided by the e5/e4 latency). Of the 162 growth curves, 5 did not have ECAPs larger than 20 μ V and were not included in further analysis. Differences in latency between ECAPs elicited with both e3/e4 and e4/e5 SCS and collected after day 1 were made for the 68 of 72 growth curves (i.e., 4 differences were excluded because at least one of growth curves did not have the minimum size ECAP).

Statistics

Summary statistics are reported as mean \pm standard error unless otherwise stated. PWTs of injured and non-injured limbs were compared using a paired *t*-test with an alpha value of 0.05. For statistical comparisons of each of the impedances, growth curve slopes, ECAPTs, vMTs, ECAPT: vMT ratios, and latency, the longitudinal data were fit into a generalized linear mixed-effects (GLME) model where fixed effects were variables, and the random effect was the rat. Specifically, for impedances and latency, the fixed effects included the anesthesia state, the recording configuration, and the day post implantation. For ECAPTs, vMTs, ECAPT:vMT ratios, and growth curve slope, the fixed effects included the anesthesia state, the PW, and the day post implantation. All fixed and random effects were categorical variables for subsequent comparison tests. Additional information and summary variance statistics of each model can be found in the [Supplementary Material](#). After fitting each model, estimated marginal means (emmeans function in MATLAB; Hartman, n.d.) were used for comparisons between specific variables (e.g., comparing between days or between pulse widths), with *p*-values reported after applying the Bonferroni correction for multiple comparisons.

Results

Impedances, ECAPs, and vMTs were recorded across 16 days in nine rats that were chronically implanted with a hexapolar epidural lead. Following our traditional SNI-SCS approach, anesthetized recordings were performed from day 0 onward, along with awake recordings from day 1 onward, to evaluate effect of chronic healing (days 1–7), nerve injury (days 7–14), and continuous DTMP-SCS (days 14–16). For the 5 animals with post-mortem imaging, three had the most rostral contact on T13 with the lead spanning caudally to approximately the bottom of L2 or the top of L3. For the two remaining rats with imaging, the lead was placed caudally by a vertebral body (with the tip near L1).



Validation of the SNI model

As seen in Figure 3A, the mean paw withdrawal threshold (PWT) of the injured limbs (18.7 ± 1.9 g) was significantly reduced ($p < 0.0001$) relative to the mean PWT of the non-injured ones (64.4 ± 6.2 g). All animals developed mechanical hypersensitivity, as defined by the PWT ratios for the injured limb being less than 70% of the non-injured limb. As seen in Figure 3 for all animals, the ratio of PWTs (injured: non-injured) limb was $31 \pm 4\%$.

Impedance stability over time

Impedances between neighboring electrodes, with the configuration shown in Figure 4A, indicated no breakages occurred for any of the 9 animals over the course of the experiment. Comparing over time (Figure 4B), impedances collected on day 1 were significantly lower compared to day 14 and 16 ($P < 0.002$). Impedances were stable from day 7 onward, with no significant differences between day 7, 14, and 16. Mean impedances were significantly lower for awake conditions than for anesthetized conditions ($P < 0.02$) (Figure 4C) by 80 ± 31 Ohms. Impedances were also significantly lower for the recording (i.e., most rostral) electrode pair compared to the other electrode pairs ($P < 0.001$) by at least 319 ± 44 Ohms, when comparing e0/e1 impedances to

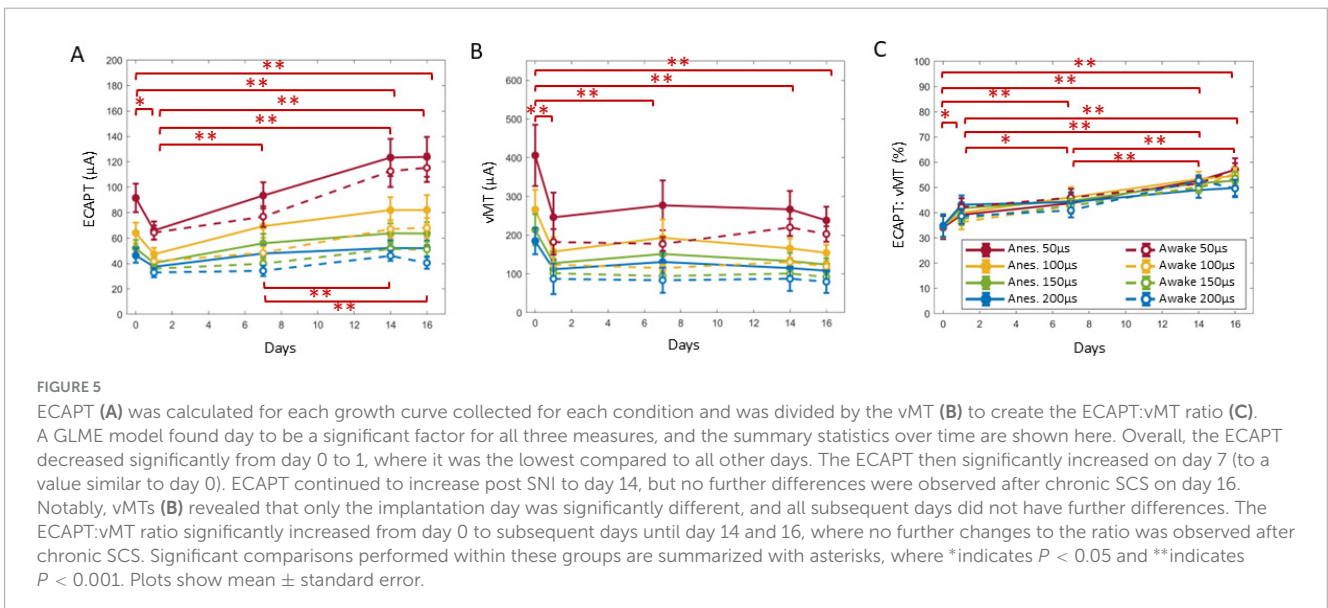
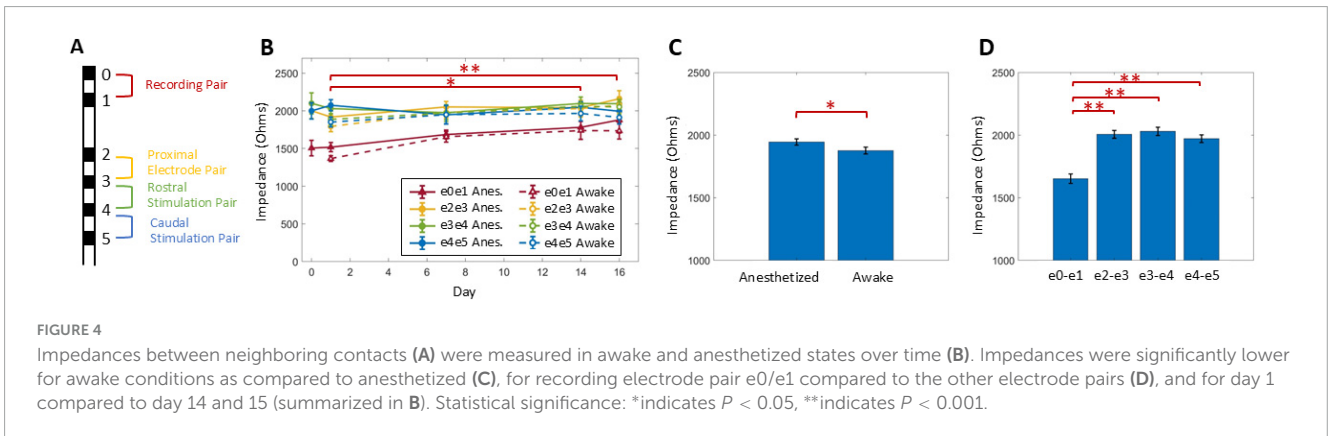
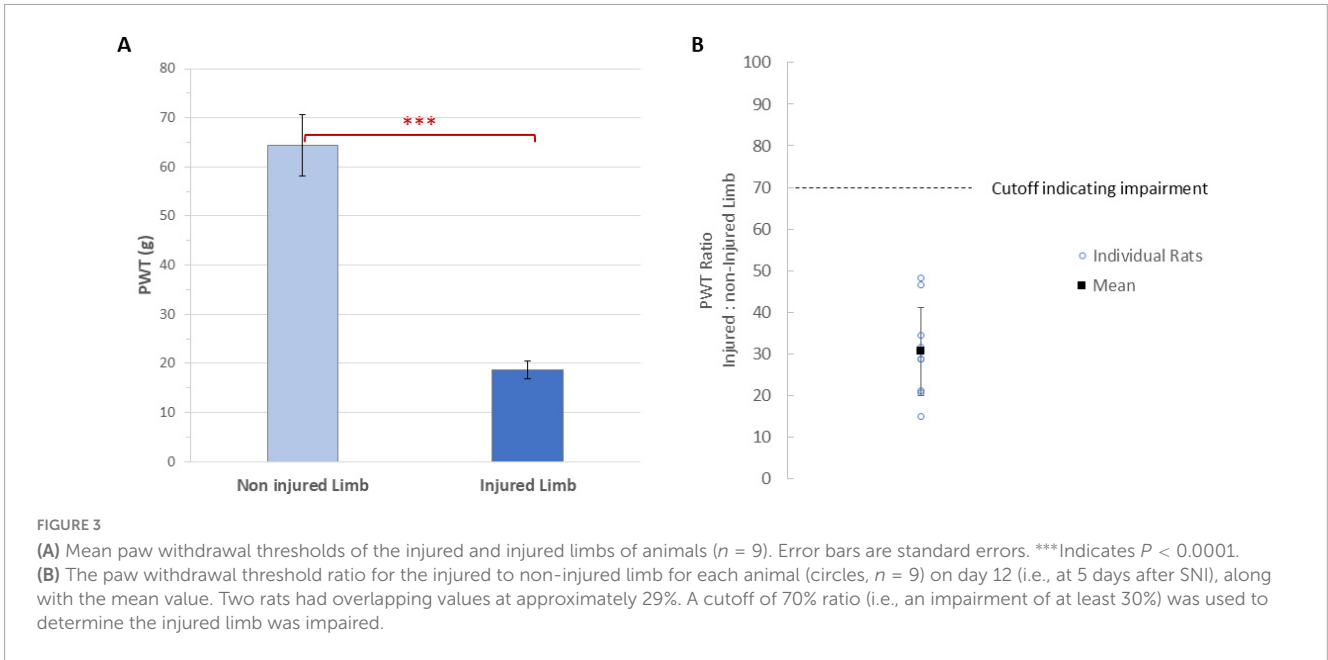
e4/e5. No further significant differences were observed between the proximal electrode pair, the rostral stimulation pair, or the caudal stimulation pair (Figure 4D).

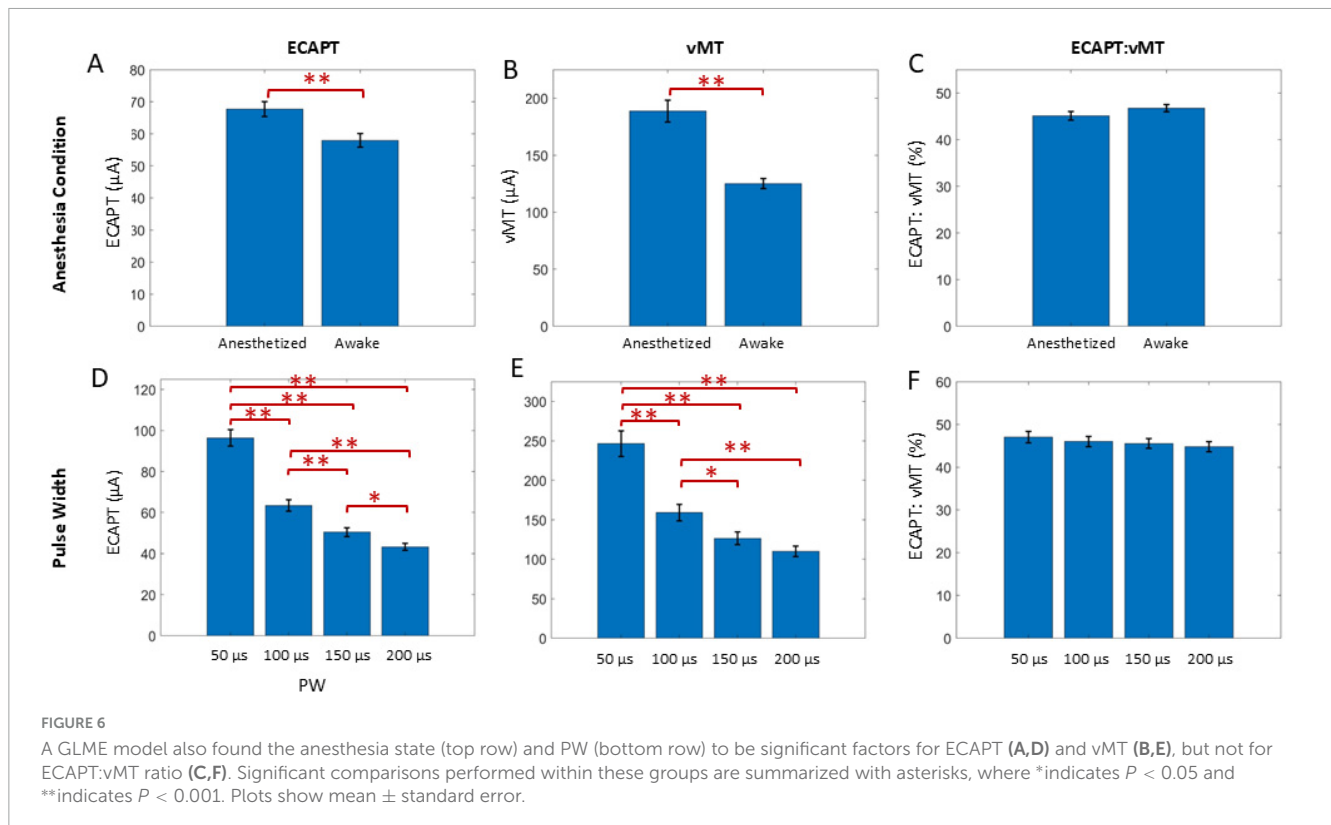
Relationship between ECAPTs and vMTs

ECAPs were observed in all nine rats for all conditions tested for all 16 days. The confidence interval (CI) of ECAPTs was under 5μ A for 91% of growth curves and under 15μ A for 98% of growth curves analyzed by the algorithm ($n = 640$ growth curves total, after excluding 7 curves that were manually corrected).

Across all animals, ECAPT significantly varied over time (Figure 5A), anesthesia state (Figure 6A) and PW (Figure 6D). Specifically, ECAPTs at day 0 were significantly greater than at day 1 ($P < 0.004$), and smaller than at day 14 or day 16 ($P < 0.001$). By day 7 ECAPTs had increased to be similar to those measured at day 0, and then continued to increase at day 14 and day 16 ($P < 0.001$), with no significant differences were observed before (day 14) and after application of SCS (day 16). Compared to recordings performed under anesthesia, awake ECAPTs were significantly lower ($P < 0.001$). As expected, ECAPTs decreased with increasing PW.

In terms of motor activation, vMTs were significantly higher on day 0 than at subsequent days ($P < 0.001$), with no further





significant differences noted in the chronic recordings (Figure 5B). Similar to ECAPTs, vMTs were significantly lower in awake animals ($P < 0.001$) (Figure 6B) and with increasing PWs (Figure 6E).

To compare the relationship between the changes in neural and muscle activation, the ECAPT:vMT ratio was calculated and compared across recording conditions. Notably, there were significant differences detected over time (Figure 5C). The ECAPT: vMT ratio was lowest for day 0 at an average of $35 \pm 2\%$ ($n = 72$ growth curves across all conditions), and progressively increased to $40 \pm 1\%$, $44 \pm 1\%$, $51 \pm 1\%$, and $54 \pm 1\%$, on days 1, 7, 14, and 16 ($n = 143$ – 144 growth curves each), with differences across successive measurement being significant for all but the last two measurement (day 14 and 16). No significant differences were detected between anesthesia/awake state or PW ($P > 0.05$) (Figures 6C,F), indicating that these conditions had similar effects on neural and muscle activation.

Slope of growth curves

In addition to ECAPTs, the calculated slopes of the growth curves were also analyzed (Figure 7). Comparing over time (Figure 7A), slopes at day 0 and 1 were significantly different from the ones at day 7 and onward ($P < 0.001$). No significant differences were observed between slopes at days 7, 14, or 16, indicating no effect from SNI (day 7 vs. day 14) or SCS (day 14 vs. day 16), and similarly there were no significant differences detected with anesthesia state (Figure 7B). The slope was most shallow for the 50μ s PW ($P < 0.01$) compared to the longer PWs, with no

further significant differences between the 100, 150, and 200 μ s PWs (Figure 7C).

Latency of ECAPs

The latency of N1 was calculated for the first ECAP that exceeded 20μ V within a growth curve in response to stimulation at 50μ s PW (Figure 8). Latency significantly decreased from day 0 to 1 ($P < 0.004$), but no further differences were observed across days (Figure 8A) or with anesthesia condition (Figure 8B). The caudal stimulation pair e4/e5 had significantly longer latencies than the rostral stimulation pair e3/e4 by $53 \pm 9 \mu$ s ($P < 0.001$). Averaging across all conditions recorded on days 1–16, the conduction velocity (CV) of ECAPs was 40 ± 1.4 m/s ($n = 69$) when stimulating with the caudal stimulation pair (e4/e5).

Discussion

In this study, a common SNI-SCS model approach for neuropathic pain was used in anesthetized and awake rodents to explore changes in electrode impedances and both neural and muscular evoked activity over time. These recordings—with the animals serving as their own controls—enabled comparison of the effects of acute healing on day 1 post lead implantation, chronic healing on day 7, neural injury on day 14 (i.e., 7 days after SNI), and after continuous DTMP-SCS on day 16. After 5 days of SNI induction, all animals developed mechanical allodynia with an average of 70% decrease in paw withdrawal thresholds, similar to impairments previously observed with this model (Vallejo et al.,

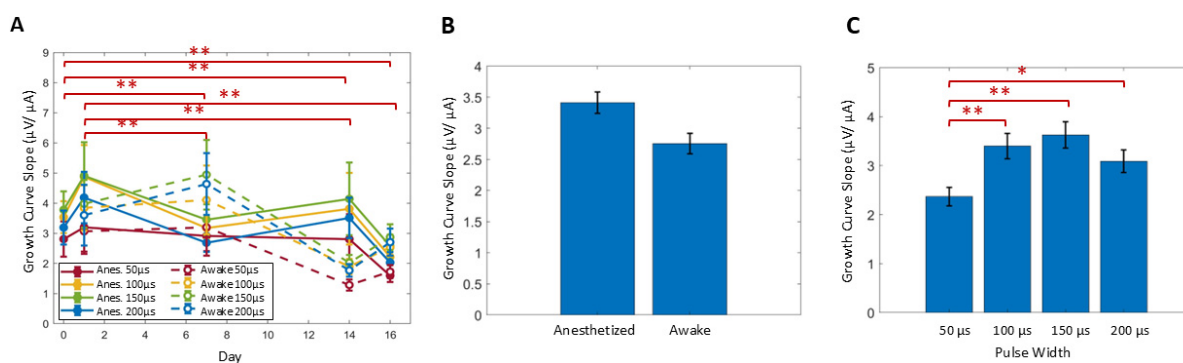


FIGURE 7
The slope of the growth curve was analyzed across days (A), relative to anesthesia conditions (B) and among stimulus PWs (C). Significant comparisons performed within these groups are summarized with asterisks, where * indicates $P < 0.05$ and ** indicates $P < 0.001$. Plots show mean \pm standard error.

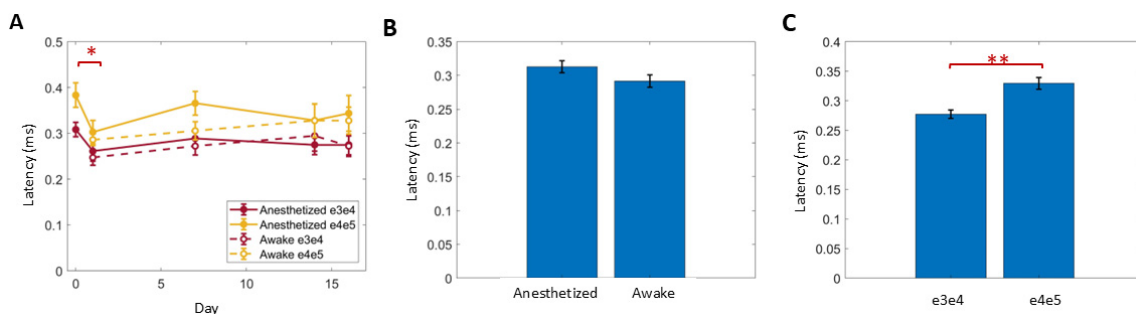


FIGURE 8
The latency of ECAPs just above 20 μ V in response to 50 Hz stimuli with 50 μ s PW was analyzed across days (A), relative to anesthesia conditions (B) and two different stimulus locations (C). Significant comparisons performed within these groups are summarized with asterisks, where * indicates $P < 0.05$ and ** indicates $P < 0.001$.

2020). The implications of these findings are discussed further below.

Impedances and the electrode-tissue interface

In this work, impedances significantly increased from day 1 compared to day 14 and 16, though, no significant differences were noted from day 7 onward. Combined with the vMT and ECAPT changes noted from day 0 to 1, these observations suggest electrode-tissue interface maturation was ongoing at least through and beyond day 1 but had stabilized by day 7. Different physiological processes specific to the implanted lead location, geometry, and materials drive the maturation of the electrode-tissue interface in both the acute, post-surgical healing phase as well as the longer term, chronic healing phase. In the acute phase, a host of factors—primarily mediated by microglia—contribute to the inflammatory response at the electrode-tissue interface as blood and edema are cleared from the surgical site (Carnicer-Lombarte et al., 2021). After some days, healing transitions to the chronic phase, where astrocytes encapsulate the implant over the span of weeks to months and form a fibrotic layer. These processes can manifest in a change in the electrode impedance over

time (Arle et al., 2014). While few prior reports of chronic SCS electrode impedance changes in rats exist, a study using titanium-nitride electrodes (versus the clinically relevant Pt-Ir electrodes used in this work) reported an initial impedance increase over the first 2 weeks post-implant followed by stable impedances thereafter for an additional 14 weeks (Garcia-Sandoval et al., 2018). Clinically, the impedances of SCS electrodes—when placed in the high thoracic spine to treat angina—were shown to decrease day 1 after implantation and stabilize within 1 month post-implant (Andersen, 1997). These impedance shifts inherently change the conductivity of the neural interface in a frequency-specific manner characterized by the Randles equivalent circuit (Randles, 1947), and are noted for both a variety of materials (Franks et al., 2005) and implant locations (both central and peripheral) (Straka et al., 2018); changes to the morphology and amplitude of the recorded ECAP may result if the signal amplifier is sensitive to these impedance shifts.

In addition to these biotic factors, the impedances verified that no breakages in the electrodes occurred throughout the experimental timeline. Two additional significant trends in impedances were evident that may be specific to this approach. First, the impedance was significantly higher while under anesthesia, which may be due to both changes in animal position and systemic effects of the isoflurane. Animals in awake states

were upright in a tube and standing on four feet, while animals under anesthesia were prone with limbs extended. Isoflurane also results in peripheral vasodilation (Constantinides et al., 2011) and decreased serum ion concentrations (Goldberg et al., 1996), factors that can influence impedance measurements. Secondly, impedances were significantly lower for the recording electrode pair than the other electrode pairs. This may be due to the relative distance between contacts, since conductive surfaces—even if they are not electrically connected to other elements in the system— influence the distribution of electrical fields in an electrolytic medium (Single and Scott, 2018).

Neural activation over time

Comparing to previous work, the ECAPT:vMT ratio of $35 \pm 2\%$ on the implantation day was similar to our previous study using similar parameters (Cedeño et al., 2023b). After day 1, the ECAPT:vMT ratio increased to $40 \pm 1\%$, corresponding to vMTs being 2.5 times larger than ECAPTs—similar to values reported of 35% in acute studies (Dietz et al., 2022) and approximately 32–45% up to 2 days post implantation (Versantvoort et al., 2024). We further observed novel findings that the ratio increased over time to $54 \pm 1\%$ on day 16. Overall, these values are similar to prior reports suggesting paresthesia thresholds occur at 40–50% of MT for animals with neuropathic pain models (Shechter et al., 2013; Song et al., 2014; Cedeño et al., 2023a).

Novel results in this study allow the investigation of neural activation acutely and compare that to a longer term chronic healing as observed on day 7. Differences in ECAPTs, vMTs, the ECAPT:vMT ratio, and latency of ECAP were observed between day 0 and 1, indicative that day 0 data may have been influenced by the longer anesthesia period and surgical trauma. Thus, data collection on day 1 is critical in both demonstrating the plainly evident differences even within a small acute healing period and distinguishing these changes from longer term healing. By day 7, impedances and motor thresholds stabilized, suggesting that further changes in ECAPT and ECAPT:vMT ratio are not likely due to long-term healing effects. Similarly, the latency for a 20 μ V ECAP had also stabilized for day 1 onward. The initial post-trauma (surgical or otherwise) latency prolongation likely represents a common finding across species for many types of evoked potentials. In guinea pigs, for instance, prolonged latencies are seen in auditory brainstem response post-acoustic trauma and in auditory nerve ECAPs post-surgical trauma; in both instances, the latency prolongation resolves after several days (Gourévitch et al., 2009; Ramekers et al., 2022).

The changes in ECAPT and ECAPT:vMT ratio over time contrast that of vMT, which exhibited no further significant changes after day 0. As such, the significant changes in ECAPT:vMT ratio both from day 1 and 7 onward are attributable solely to shifts in the ECAPTs versus shifts in the electrode impedance or vMT. One intriguing explanation for this observation is modulation of neural excitation in the dorsal columns by the SNI model. Notably, this effect stabilized, and no further differences were observed after the application of SCS, at least within the 2-day period of this study. The stability of this ratio after continuous SCS is relevant translationally as it suggests that DTMP does not

alter the electrophysiology of the dorsal column A β fibers from which ECAPs originate. DTMP, which is shown to have significant improvement of mechanical hypersensitivity in rats compared to low-rate or high-rate stimulation alone, has been shown to modify the expression of glial genes toward a non-pain state (Vallejo et al., 2020), but the effect on neural excitation had not been studied previously. Moreover, this result indicated that dosing is consistent over time, given that SCS in translational models is typically dosed relative to vMT and not further adjusted after therapy begins. In contrast, changes in this ratio after SCS would have indicated that therapy would require adjustment in amplitude over time to achieve consistent dosing. The similarity in ECAPT:vMT ratio before and after continuous SCS agrees with previous findings of consistent sensory thresholds in similar rat SNI models after 3 days of either low or high frequency stimulation (Shechter et al., 2013).

Effect of pulse width on neural activation

We confirmed the effect of PW from 50 to 200 μ s on growth curves trends across time and neural activation metrics. As expected from the classic strength-duration curve relationship (Brunel and Van Rossum, 2007), an increase in PW decreased ECAPT and vMT as more charge was delivered to the tissue. Similar to previous work (Cedeño et al., 2023b; Versantvoort et al., 2024), the PW did not affect the ECAPT: vMT ratio up to 16 days after implantation. While ECAPs were observed for all PWs tested in this study, the stimulation artifact elicited by the longer PWs partially effaced the N1 feature within the ECAP, especially in response to the 200 μ s PW. The artifact obstruction may have had a small effect on the slope of the growth curve, given that the 200 μ s PW results were on average lower (but not significantly) than with the 100 or 150 μ s PWs.

Effects of anesthesia

In this study, the anesthetic agent (isoflurane) significantly increased impedances, ECAPTs, and vMTs, but had no effect on ECAPT: vMT ratios, the slope of the growth curve, or the latency of a 20 μ V ECAP. The effect of isoflurane increasing motor thresholds has previously been described in rats approximately 1 day (Dietz et al., 2022) and 1 month (Yang et al., 2011) after implantation of an SCS lead. Overall, isoflurane has a depressive effect of muscle activity across a variety of preclinical models, where the anesthesia significantly reduces compound muscle action potentials (CMAPs) in amplitude in mice (Osuchowski et al., 2009) after 5 min of exposure. Similar results have been noted in cats (Yamada et al., 1995), Nubian goats (Andel et al., 2000) and humans (Rohde et al., 2003).

In addition to blocking motor responses, isoflurane has been shown to decrease neural excitability of neurons in the dorsal horn (Yang et al., 2021) by binding to GABA and glycine receptors (Grasshoff and Antkowiak, 2006). In ovines, ECAPT and growth curve slopes were lower for awake conditions than under isoflurane when recorded on the same day (Goodman et al., 2020). In contrast to our results where ECAPTs were lower in awake states, Dietz et al found that ECAPTs were comparable between conditions (Dietz

et al., 2022). Notably, in that study, unanesthetized recordings were collected at least 4 h after anesthetized condition, which was taken immediately after implantation. In addition, while we did not observe difference in latencies (and thus conduction velocities) in spinal ECAPs between anesthetic states, previous nerve conduction studies in mice found that isoflurane decreases nerve conduction after 5 min of exposure compared to awake conditions (Osuchowski et al., 2009), though the impact on CV is less in comparison to other anesthetics (Oh et al., 2010). Such differences in latencies or CV may require leads with greater site separation than the 1-mm inter-electrode spacing used here to detect differences in future research.

Latencies and conduction velocity

The conduction velocities recorded here averaged at 40 ± 1.4 m/s, similar to orthodromically recorded ECAPs in previous studies (Dietz et al., 2022). These results suggest that ECAPs from large, myelinated fibers were acquired. No differences in latencies after day 1 or between anesthesia condition was observed, contrasting a prior report of antidromic CVs being significantly slower in SNI animals as compared to sham (Versantvoort et al., 2024). These differences may be due to inter-animal differences, especially as only 4–5 animals were allocated per group in the prior study, or due to the limited sampling resolution of $33 \mu\text{s}$ (as compared to the resolution of $25 \mu\text{s}$ in this study). In contrast, this study used only the latencies from one ECAP amplitude for consistency (i.e., just exceeding $20 \mu\text{V}$) to assess latency differences across different animals and conditions.

Clinical translation

These results highlight acute changes in the neural interface with translational impacts. Accordingly, caution is inculcated for the clinician using SCS systems that rely on stability of the electrode-tissue interface—such as ECAP-controlled, SCS systems that deliver closed-loop paresthesia at a specific ECAP amplitude (Russo et al., 2018)—as this interface is still maturing perioperatively. Establishing parameters for closed-loop therapy while these changes are underway may result in poor dose control or un-optimized therapy for some patients. For example, as the ratio between neural and motor threshold increases, this would likely be translated to differences in neural and sensory thresholds. Additionally, systems that use a template for ECAP identification may need adjustments as the morphology of the ECAP changes with N1 latency decreases. In humans, these factors may be acutely compounded, where some contacts have high impedances immediately post implantation due to blood or air bubbles that are then resolved in subsequent days. Importantly, the stability in ECAPT as well as ECAPT:vMT after 2 days of continuous DTMP in this study suggests that neural excitability does not change further—a clinically meaningful outcome, as further modulation would likely indicate therapy reprogramming. Similar to work demonstrating how small changes in distance between the lead contacts and the spinal

cord impacts neural activation (Brucker-Hahn et al., 2023), future computational modeling work could illuminate how differences in the electrode-tissue interface impacts the activation of A β fibers.

Study limitations

The study was structured to mimic previous SNI studies, where each animal served as its own control for pre-SNI (days 1–7), post SNI (day 14), and post SCS (day 16). The limitation in this approach is that the stability of ECAPs from days 14 + was not evaluated without the influence of SNI. However, a recent study compared animals with and without SNI injury for 2 days post SCS and did not find significant differences in the MT:ECAPT ratios between sham and SNI animals (Versantvoort et al., 2024). Moreover, the limited sample size of 9 animals, while similar to previous work and is sufficient to validate the SNI model, limits some statistical comparisons in which experimental variance was larger (such as latency in awake versus anesthetized animals). Another limitation in this study was that the effect of continuous SCS was only taken over 2 days, which was chosen to follow previous studies investigating the behavioral effects and mechanism of action of DTMP (Cedeño et al., 2020, 2023a; Vallejo et al., 2020). Future studies should explore longer-term effects of DTMP-SCS on ECAPs. Additional methodological constraints include that PWTs were only measured 5 days post-SNI to validate that the animals had developed the model, and did not measure them pre- and post-SCS. This approach, which reduced the number of experimental interventions, used previous literature (Decosterd and Woolf, 2000) and our own experience (Tilley et al., 2015; Vallejo et al., 2020) to validate the sustainability of the model. Additionally, there were some practical limitations of the recordings, including placing the reference needle and restraining the animal in a tube to minimize movement artifacts. However, the impact on elicited neural activity is likely minimal given the lack of significant differences detected between anesthetized states for the ECAPT: vMT ratios, the slope of the growth curve, or the latency of a $20 \mu\text{V}$ ECAP. Finally, it was not possible to collect x-ray images for all animals in the study, although for the first 5 animals lead placement was confirmed to be within one vertebral body of the target T13, suggesting that this electrode array configuration and surgical technique enabled consistent placement.

Conclusion

This study provides novel evidence demonstrating the feasibility of recording spinal ECAPs with clinically relevant electrode configurations in rats over the span of weeks. Over time, the relationship between ECAPT and MTs varies both due to healing as well as nerve injury, and this provides crucial insights into SCS dosing for translational research. This approach could be leveraged for a variety of future studies searching to elucidate mechanisms of action and neurophysiological changes underpinning SCS therapies.

Data availability statement

The datasets presented in this article are not readily available because the datasets are the property of Medtronic plc. Requests to access the datasets should be directed to david.a.dinsmoor@medtronic.com.

Ethics statement

The animal study was approved by Institutional Animal Care and Use Committee at Illinois Wesleyan University. The study was conducted in accordance with the local legislation and institutional requirements.

Author contributions

DC: Conceptualization, Methodology, Supervision, Writing – review & editing. RV: Conceptualization, Methodology, Supervision, Writing – review & editing. DP: Conceptualization, Data curation, Investigation, Methodology, Writing – review & editing. JW: Resources, Supervision, Writing – review & editing. LL: Conceptualization, Formal Analysis, Funding acquisition, Investigation, Resources, Supervision, Writing – review & editing. DD: Conceptualization, Funding acquisition, Investigation, Methodology, Resources, Supervision, Writing – original draft, Writing – review & editing. MS: Conceptualization, Data curation, Formal Analysis, Investigation, Methodology, Writing – original draft, Writing – review & editing.

Funding

The author(s) declare that financial support was received for the research and/or publication of this article. This study was funded by the Medtronic plc.

References

- Al-Kaisy, A., Baranidharan, G., Palmisani, S., Pang, D., Will, O., Wesley, S., et al. (2020). Comparison of paresthesia mapping to anatomical placement in burst spinal cord stimulation: Initial trial results of the prospective, multicenter, randomized, double-blinded, crossover, CRISP study. *Neuromodulation* 23, 613–619. doi: 10.1111/ner.13104
- Andel, H., Bayer, G. S., Ciovica, R., Monsivais, J., Basco, M., Zimpfer, M., et al. (2000). Depressive effect of isoflurane on motor evoked potentials in the Nubian goat. *Can. J. Anaesth.* 47, 81–86. doi: 10.1007/BF03020739
- Andersen, C. (1997). Time dependent variation of stimulus requirements in spinal cord stimulation for angina pectoris. *Pacing Clin. Electrophysiol.* 20(2 Pt 1), 359–363. doi: 10.1111/j.1540-8159.1997.tb06183.x
- Arle, J. E., Carlson, K. W., Mei, L., and Shils, J. L. (2014). Modeling effects of scar on patterns of dorsal column stimulation. *Neuromodulation* 17, 320–333; discussion 333. doi: 10.1111/ner.12128
- Brucker-Hahn, M. K., Zander, H. J., Will, A. J., Vallabh, J. C., Wolff, J. S., Dinsmoor, D. A., et al. (2023). Evoked compound action potentials during spinal cord stimulation: Effects of posture and pulse width on signal features and neural activation within the spinal cord. *J. Neural Eng.* 20, 1741–2552. doi: 10.1088/1741-2552/accca4
- Brunel, N., and Van Rossum, M. C. W. (2007). Quantitative investigations of electrical nerve excitation treated as polarization. *Biol. Cybern.* 97, 341–349. doi: 10.1007/s00422-007-0189-6
- Carnicer-Lombarte, A., Chen, S. T., Malliaras, G. G., and Barone, D. G. (2021). Foreign body reaction to implanted biomaterials and its impact in nerve neuroprosthetics. *Front. Bioeng. Biotechnol.* 9:622524. doi: 10.3389/fbioe.2021.622524
- Cedeño, D. L., Kelley, C. A., and Vallejo, R. (2023a). Effect of stimulation intensity of a differential target multiplexed SCS program in an animal model of neuropathic pain. *Pain Pract.* 23, 639–646. doi: 10.1111/papr.13235
- Cedeño, D. L., Smith, W. J., Kelley, C. A., and Vallejo, R. (2020). Spinal cord stimulation using differential target multiplexed programming modulates neural cell-specific transcriptomes in an animal model of neuropathic pain. *Mol. Pain* 16:1744806920964360. doi: 10.1177/1744806920964360
- Cedeño, D. L., Vallejo, R., Kelley, C. A., Platt, D. C., Litvak, L. M., Straka, M., et al. (2023b). Spinal evoked compound action potentials in rats with clinically relevant stimulation modalities. *Neuromodulation* 26, 68–77. doi: 10.1016/j.neurom.2022.06.006

Conflict of interest

RV is a consultant for Medtronic plc. DC, RV, and DP are consultants for SGX Medical LLC. LL, MS, and DD are employees of Medtronic plc.

The remaining author declares that the research was conducted in the absence of any commercial or financial relationships that could be construed as a potential conflict of interest.

The authors declare that this study received funding from Medtronic plc. The funder had the following involvement in the study: study design, data collection and analysis, decision to publish, and preparation of the manuscript.

Generative AI statement

The authors declare that no Generative AI was used in the creation of this manuscript.

Publisher's note

All claims expressed in this article are solely those of the authors and do not necessarily represent those of their affiliated organizations, or those of the publisher, the editors and the reviewers. Any product that may be evaluated in this article, or claim that may be made by its manufacturer, is not guaranteed or endorsed by the publisher.

Supplementary material

The Supplementary Material for this article can be found online at: <https://www.frontiersin.org/articles/10.3389/fnins.2025.1577059/full#supplementary-material>

- Cedeno, D., Platt, D., Kelley, C., Williams, J., Fields, M., Petersen, C., et al. (2022). Significant relief of mechanical hypersensitivity by continuous differential target multiplexed SCS is sustained for 23 days in an animal model of persistent neuropathic pain. *Neuromodulat. Technol. Neural Interface* 25, S47–S48. doi: 10.1016/j.neurom.2022.08.055
- Chakravarthy, K., Bink, H., and Dinsmoor, D. (2020). Sensing evoked compound action potentials from the spinal cord: Novel preclinical and clinical considerations for the pain management researcher and clinician. *J. Pain Res.* 13, 3269–3279. doi: 10.2147/JPR.S289098
- Chakravarthy, K., FitzGerald, J., Will, A., Trutnau, K., Corey, R., Dinsmoor, D., et al. (2022). A clinical feasibility study of spinal evoked compound action potential estimation methods. *Neuromodulation* 25, 75–84. doi: 10.1111/ner.13510
- Constantinides, C., Mean, R., and Janssen, B. J. (2011). Effects of isoflurane anesthesia on the cardiovascular function of the C57BL/6 mouse. *ILAR J.* 52, e21–e31.
- Crosby, N. D., Weisshaar, C. L., Smith, J. R., Zeeman, M. E., Goodman-Keiser, M. D., and Winkelstein, B. A. (2015). Burst and tonic spinal cord stimulation differentially activate gabaergic mechanisms to attenuate pain in a rat model of cervical radiculopathy. *IEEE Trans. Biomed. Eng.* 62, 1604–1613. doi: 10.1109/TBME.2015.2399374
- Decosterd, I., and Woolf, C. J. (2000). Spared nerve injury: An animal model of persistent peripheral neuropathic pain. *Pain* 87, 149–158. doi: 10.1016/S0304-3959(00)00276-1
- Dietz, B. E., Mughan, D., Vuong, Q. C., and Obara, I. (2022). Electrically evoked compound action potentials in spinal cord stimulation: Implications for preclinical research models. *Neuromodulation* 25, 64–74. doi: 10.1111/ner.13480
- Franks, W., Schenker, I., Schmutz, P., and Hierlemann, A. (2005). Impedance characterization and modeling of electrodes for biomedical applications. *IEEE Trans. Biomed. Eng.* 52, 1295–1302. doi: 10.1109/TBME.2005.847523
- García-Sandoval, A., Pal, A., Mishra, A. M., Sherman, S., Parikh, A. R., Joshi-Imre, A., et al. (2018). Chronic softening spinal cord stimulation arrays. *J. Neural Eng.* 15:045002. doi: 10.1088/1741-2552/aab90d
- Goldberg, M. E., Cantillo, J., Larijani, G. E., Torjman, M., Vekeman, D., and Schieren, H. (1996). Sevoflurane versus isoflurane for maintenance of anesthesia: Are serum inorganic fluoride ion concentrations of concern? *Anesth. Analg.* 82, 1268–1272. doi: 10.1097/0000539-199606000-00029
- Goodman, M., Pilitsis, J., and Fishman, M. D. D. (2020). ECAPs in the dorsal columns of awake vs. anesthetized ovines. abstr. from north am. neuromodulation soc. 23rd annu. meet. las vegas, NV, USA. *Neuromodulation* 23:e231. doi: 10.1111/ner.13133
- Gourévitch, B., Doisy, T., Avillac, M., and Edeline, J. M. (2009). Follow-up of latency and threshold shifts of auditory brainstem responses after single and interrupted acoustic trauma in guinea pig. *Brain Res.* 1304, 66–79. doi: 10.1016/j.brainres.2009.09.041
- Grasshoff, C., and Antkowiak, B. (2006). Effects of isoflurane and enflurane on GABAA and glycine receptors contribute equally to depressant actions on spinal ventral horn neurones in rats. *Br. J. Anaesth.* 97, 687–694. doi: 10.1093/bja/ael239
- Hartman, J. (n.d.). *emmeans v1.0.0. github*. Available online at: <https://github.com/jackatta/estimated-marginal-means> (accessed August 17, 2023).
- Martinov, T., Mack, M., Sykes, A., and Chatterjea, D. (2023). Measuring changes in tactile sensitivity in the hind paw of mice using an electronic von Frey apparatus. *J. Vis. Exp.* 82:e51212. doi: 10.3791/51212
- Oh, S. S., Hayes, J. M., Sims-Robinson, C., Sullivan, K. A., and Feldman, E. L. (2010). The effects of anesthesia on measures of nerve conduction velocity in male C57Bl6/J mice. *Neurosci. Lett.* 483, 127–131. doi: 10.1016/j.neulet.2010.07.076
- Osuchowski, M. F., Teener, J., and Remick, D. (2009). Noninvasive model of sciatic nerve conduction in healthy and septic mice: Reliability and normative data. *Muscle Nerve* 40, 610–616. doi: 10.1002/mus.21284
- Pilitsis, J. G., Chakravarthy, K. V., Will, A. J., Trutnau, K. C., Hageman, K. N., Dinsmoor, D. A., et al. (2021). The evoked compound action potential as a predictor for perception in chronic pain patients: Tools for automatic spinal cord stimulator programming and control. *Front. Neurosci.* 15:673998. doi: 10.3389/fnins.2021.673998
- Ramekers, D., Benav, H., Klis, S. F. L., and Versnel, H. (2022). Changes in the electrically evoked compound action potential over time after implantation and subsequent deafening in guinea pigs. *J. Assoc. Res. Otolaryngol.* 23, 721–738. doi: 10.1007/s10162-022-00864-0
- Randles, J. E. B. (1947). Kinetics of rapid electrode reactions. *Faraday Discuss.* 1, 11–19. doi: 10.1039/DF9470100011
- Reddy, C. G., Miller, J. W., Abode-Iyamah, K. O., Safayi, S., Wilson, S., Dalm, B. D., et al. (2018). Ovine model of neuropathic pain for assessing mechanisms of spinal cord stimulation therapy via dorsal horn recordings, von Frey filaments, and gait analysis. *J. Pain Res.* 11, 1147–1162. doi: 10.2147/JPR.S139843
- Rohde, V., Krombach, G. A., Baumert, J. H., Kreitschmann-Andermahr, I., Weinzierl, M., and Gilsbach, J. M. (2003). Measurement of motor evoked potentials following repetitive magnetic motor cortex stimulation during isoflurane or propofol anaesthesia. *Br. J. Anaesth.* 91, 487–492. doi: 10.1093/bja/aeg224
- Russo, M., Cousins, M. J., Brooker, C., Taylor, N., Boesel, T., Sullivan, R., et al. (2018). Effective relief of pain and associated symptoms with closed-loop spinal cord stimulation system: Preliminary results of the avalon study. *Neuromodulation* 21, 38–47. doi: 10.1111/ner.12684
- Sagalajev, B., Zhang, T., Abdollahi, N., Yousefpour, N., Medlock, L., Al-Basha, D., et al. (2024). Absence of paresthesia during high-rate spinal cord stimulation reveals importance of synchrony for sensations evoked by electrical stimulation. *Neuron* 112, 404–420.e6. doi: 10.1016/j.neuron.2023.10.021
- Salatino, J. W., Ludwig, K. A., Kozai, T. D. Y., and Purcell, E. K. (2017). Glial responses to implanted electrodes in the brain. *Nat. Biomed. Eng.* 1, 862–877. doi: 10.1038/s41551-017-0154-1
- Sharma, M., Bhaskar, V., Yang, L., FallahRad, M., Gebodh, N., Zhang, T., et al. (2023). Novel evoked synaptic activity potentials (ESAPs) elicited by spinal cord stimulation. *eNeuro* 10:ENEURO.0429-22.2023. doi: 10.1523/ENEURO.0429-22.2023
- Shechter, R., Yang, F., Xu, Q., Cheong, Y. K., He, S. Q., Sdrulla, A., et al. (2013). Conventional and kilohertz-frequency spinal cord stimulation produces intensity- and frequency-dependent inhibition of mechanical hypersensitivity in a rat model of neuropathic pain. *Anesthesiology* 119, 422–432. doi: 10.1097/ALN.0b013e31829bd9e2
- Shepherd, R. K., Villalobos, J., Burns, O., and Nayagam, D. A. X. (2018). The development of neural stimulators: A review of preclinical safety and efficacy studies. *J. Neural Eng.* 15:041004. doi: 10.1088/1741-2552/aac43c
- Single, P., and Scott, J. (2018). Cause of pulse artefacts inherent to the electrodes of neuromodulation implants. *IEEE Trans. Neural Syst. Rehabil. Eng.* 26, 2078–2083. doi: 10.1109/TNSRE.2018.2870169
- Song, Z., Viisanen, H., Meyerson, B. A., Pertovaara, A., and Linderöth, B. (2014). Efficacy of kilohertz-frequency and conventional spinal cord stimulation in rat models of different pain conditions. *Neuromodulation* 17, 226–334; discussion 234–235. doi: 10.1111/ner.12161
- Straka, M. M., Shafer, B., Vasudevan, S., Welle, C., and Rieth, L. (2018). Characterizing longitudinal changes in the impedance spectra of in-vivo peripheral nerve electrodes. *Micromachines (Basel)* 9:587. doi: 10.3390/mi9110587
- Tilley, D. M., Vallejo, R., Kelley, C. A., Benyamin, R., and Cedeño, D. L. (2015). A continuous spinal cord stimulation model attenuates pain-related behavior in vivo following induction of a peripheral nerve injury. *Neuromodulation* 18, 171–186; discussion 176. doi: 10.1111/ner.12280
- Vallejo, R., Kelley, C. A., Gupta, A., Smith, W. J., Vallejo, A., and Cedeño, D. L. (2020). Modulation of neuroglial interactions using differential target multiplexed spinal cord stimulation in an animal model of neuropathic pain. *Mol. Pain* 16:1744806920918057. doi: 10.1177/1744806920918057
- Versantvoort, E. M., Dietz, B. E., Mughan, D., Vuong, Q. C., Luli, S., and Obara, I. (2024). Evoked compound action potential (ECAP)-controlled closed-loop spinal cord stimulation in an experimental model of neuropathic pain in rats. *Bioelectr. Med.* 10:2. doi: 10.1186/s42234-023-00134-1
- Wang, D., Lee, K. Y., Lee, D., Kagan, Z. B., and Bradley, K. (2022). Low-Intensity 10 kHz spinal cord stimulation reduces behavioral and neural hypersensitivity in a rat model of painful diabetic neuropathy. *J. Pain Res.* 15, 1503–1513. doi: 10.2147/JPR.S358427
- Yamada, H., Transfeldt, E. E., Tamaki, T., Nishiura, H., Taylor, B. A., Torres, F., et al. (1995). General anesthetic effects on compound muscle action potentials elicited by single or dual spinal cord stimulation. *J. Spinal Disord.* 8, 157–162.
- Yang, D., Yang, X. J., Shao, C., and Yang, K. (2021). Isoflurane decreases substantia gelatinosa neuron excitability and synaptic transmission from periphery in the rat spinal dorsal horn. *Neuroreport* 32, 77–81. doi: 10.1097/WNR.0000000000001557
- Yang, F., Carteret, A. F., Wacnik, P. W., Chung, C. Y., Xing, L., Dong, X., et al. (2011). Bipolar spinal cord stimulation attenuates mechanical hypersensitivity at an intensity that activates a small portion of A-fiber afferents in spinal nerve-injured rats. *Neuroscience* 199, 470–480. doi: 10.1016/j.neuroscience.2011.09.049